From the synthesis of hBN crystals to their use as nanosheets in van der Waals heterostructures

Camille Maestre, Yangdi Li, Vincent Garnier, Philippe Steyer, Sébastien Roux, Aexandre Plaud, Annick Loiseau, Julien Barjon, Lei Ren, Cedric Robert, et al.

From the synthesis of hBN crystals to their use as nanosheets in van der Waals heterostructures

2D Materials

PAPER

From the synthesis of hBN crystals to their use as nanosheets in van der Waals heterostructures

Camille Maestre[1,2], Yangdi Li[1,2], Vincent Garnier[2], Philippe Steyer[2], Sébastien Roux[3,4], Alexandre Plaud[3,4], Annick Loiseau[3], Julien Barjon[4], Lei Ren[5], Cedric Robert[5], Bo Han[5], Xavier Marie[5], Catherine Journet[1,*] and Berangere Toury[1,*]

[1] Laboratoire des Multimatériaux et Interfaces (LMI), UMR CNRS 5615, University Lyon, Université Claude Bernard Lyon 1, F-69622 Villeurbanne, France
[2] UCBL, CNRS, MATEIS, UMR 5510, Université de Lyon, INSA Lyon, 7 Avenue Jean Capelle, Villeurbanne 69621 CEDEX, France
[3] Laboratoire d'Etude des Microstructures, ONERA-CNRS, Université Paris-Saclay, BP 72, F-92322 Châtillon Cedex, France
[4] Université Paris-Saclay, UVSQ, CNRS, GEMaC, F-78000 Versailles, France
[5] Laboratoire de Physique et Chimie des Nano-Objets (LPCNO), UMR CNRS 5215, Institut National des Sciences Appliquées, 135 Avenue de Rangueil, F-31077 Toulouse Cedex 4, France
* Authors to whom correspondence should be addressed.

E-mail: catherine.journet@univ-lyon1.fr **and** berangere.toury@univ-lyon1.fr

Keywords: synthesis, hBN, crystals, nanosheets

OPEN ACCESS

RECEIVED
19 January 2022

REVISED
28 April 2022

ACCEPTED FOR PUBLICATION
3 May 2022

PUBLISHED
18 May 2022

Abstract

In the wide world of 2D materials, hexagonal boron nitride (hBN) holds a special place due to its excellent characteristics. In addition to its thermal, chemical and mechanical stability, hBN demonstrates high thermal conductivity, low compressibility, and wide band gap around 6 eV, making it a promising candidate for many groundbreaking applications and more specifically in van der Waals heterostructures. Millimeters scale hBN crystals are obtained through a disruptive dual method (polymer derived ceramics (PDC)/pressure-controlled sintering (PCS)) consisting in a complementary coupling of the PDC route and a PCS process. In addition to their excellent chemical and crystalline quality, these crystals exhibit a free exciton lifetime of 0.43 ns, as determined by time-resolved cathodoluminescence measurements, confirming their interesting optical properties. To go further in applicative fields, hBN crystals are then exfoliated, and resulting boron nitride nanosheets (BNNSs) are used to encapsulate transition metal dichalcogenides (TMDs). Such van der Waals heterostructures are tested by optical spectroscopy. BNNSs do not luminesce in the emission spectral range of TMDs and the photoluminescence width of the exciton at 4 K is in the range 2–3 meV. All these results demonstrate that these BNNSs are of high quality and relevant for future opto-electronic applications.

1. Introduction

The continuous miniaturization of mobile devices combined with their performance and speed improvements require the development of elemental components that can meet these needs. These past years, a lot of efforts have been focused on the design of two-dimensional (2D) materials, that present specific properties related to their size reduction: electronic confinement, modifying both optical and electronic properties, high surface to volume ratio that affects the mechanical and chemical properties, reduced thickness allowing interesting flexibility, and low weight. In the wide world of 2D materials, beyond graphene, transition metal dichalcogenides (TMDs) and hexagonal boron nitride (hBN) hold a special place due to their excellent characteristics, especially for optoelectronic devices [1–3]. However, it is now well established that the optical, electronic and transport properties of TMD monolayers (MLs) are strongly improved if the dielectric environment of the 2D layer is well controlled [4–8]. The best results have been obtained through encapsulation of the MLs in high quality hBN [9]. In that sense, chemical purity and crystallinity of hBN are of prime importance. Besides, a lateral size up to hundreds of microns coupled with a thickness at the nanoscale has to be taken into account for integration into these devices. To date, most of the research groups working on the physics of 2D materials based on TMDs are using

high quality hBN exfoliated from the famous crystals from NIMS laboratory in Japan [9, 10]. Those crystals are generally referred to as high pressure high temperature (HP/HT). Their exceptional quality is now well established and still unmatched. As such, the properties of NIMS crystals are often used as an ultimate reference for hBN. The high quality is preserved after mechanical exfoliation [11]. A serious bottleneck lies in their fabrication technique, which is based on severe conditions of pressure, temperature and duration, which are not easily compatible with industrial perspectives [11, 12]. Besides, the use of a non-standard and heavy equipment (i.e. a massive hydraulic press) is required, which strongly limits any upscaling or industrial production. It is worth noticing that more recently, samples demonstrating almost similar quality were achieved by an atmospheric pressure HT (AP/HT) method [12–15]. This process requires a very slow cooling at HT (a few days long) limiting once more its upscaling.

Following pioneering studies [16–18], we have recently proposed an alternative synthesis approach conducted under quite soft conditions, involving a polymer derived ceramics (PDC) route and a post-sintering process performed into a pressure-controlled furnace (PDC/pressure-controlled sintering (PCS)) [19]. With this original coupling, large and transparent hBN single crystals up to millimeter size have been obtained through softer conditions and have led to boron nitride nanosheets (BNNSs) presenting a lateral size up to few hundreds microns after exfoliation. This two-step method, which allows a BNNSs production on a larger scale and at lower cost, may represent a credible alternative to the current HP/HT source of hBN.

In this paper, we demonstrate that, whatever the considered scale, the morphology, lattice structure and chemical composition corroborate the high crystal quality and low contamination level of hBN. In search for more precise characterization technique, cathodoluminescence (CL) measurements are presented. They show that residual carbon contamination persists in PDC/PCS crystals, higher than in HP/HT ones. Yet, we show that the encapsulation of TMD MLs with BNNSs obtained by the polymer route yields excellent optoelectronic properties, very comparable to the ones achieved with the HP/HT boron nitride crystals. These results on TMD encapsulation tend to show that, application-wise, small difference is observed between both sources.

2. Methods

2.1. Samples preparation

Pure borazine is obtained from a reaction between ammonium sulfate [$(NH_4)_2SO_4$, 99% purity, Aldrich] and sodium borohydride ($NaBH_4$, 98% purity, Aldrich) in tetraglyme heated to 120 °C according to a procedure described elsewhere [20] and purified twice by distillation. The liquid state polymeric precursor is then obtained by polycondensation of borazine at 50 °C inside a pressure-sealed system under argon for 5 d, generating colorless polyborazylene (PBN) with a chemical formula $(B_{3.0}N_{3.8}H_{4.0})_n$ as given by elemental analysis. A mixture of liquid PBN and 35 wt% lithium nitride (Li_3N) is preceramized at 650 °C for 1 h under an inert atmosphere of N_2. The preceramic powder is then introduced under nitrogen into a BN crucible and thereafter transferred into a pressure-controlled furnace. The chamber is purged with three cycles (N_2 filling followed by pumping) to remove oxygen and moisture. The temperature and the pressure are both increased in 30 min up to 1800 °C and up to 180 MPa with N_2. The dwelling time is 8 h, before cooling down to room temperature and pressure release.

hBN fragments (assembly of few single-crystalline flakes) are extracted from as-grown bulk samples by sliding with tweezers.

BNNSs are obtained by exfoliation using a polydimethylsiloxane (PDMS) dry transfer and deposited onto an oxidized silicon substrate (285 nm thick SiO_2).

2.2. Optical devices preparation

The TMD based van der Waals heterostructures are fabricated by mechanical exfoliation of bulk TMD (from 2D semiconductors) and BNNs crystals using a dry-stamping technique [21]. A first layer of BNNS (bottom hBN) is mechanically exfoliated onto a freshly cleaved SiO_2/Si substrate. The deposition of the subsequent TMD ML and the second BNNS capping layer (top hBN) is obtained by repeating this procedure.

2.3. Characterization techniques

The synthesized BN materials are characterized by optical microscopy using a Zeiss Axiophot Photomicroscope as well as by scanning electron microscope (SEM) using a FEG-SUPRA Zeiss 55VP microscope operating at 800 V acceleration voltage. X-ray diffraction (XRD) is carried out with a Bruker D8 Advance diffractometer, using Cu K(α) radiation source, $\lambda = 1.540\ 60$ Å, and the Raman spectra are recorded using a Labram HR800 spectrometer (HORIBA Jobin-Yvon) with 532 nm laser excitation wavelength. X-ray photoemission spectroscopy (XPS) is performed, using a PHI Quantera SXM spectrometer with Al K(α) monochromatism radiation. Sample is kept on the holder using carbon paste. The raw XPS data are corrected using the binding energy of the C–C bond at 284.5 eV and fitted with Gaussian–Lorentzian curves. Atomis force microscopy (AFM) images are acquired by using a CSI Nano-Observer apparatus in intermittent contact mode. The deep ultra-violet (UV) spectroscopy spectra were recorded at room temperature in a

JEOL7001F field-emission-gun SEM coupled to a Horiba Jobin-Yvon CL detection system as described in [22, 23]. Photoluminescence (PL) and reflectance measurements were performed in a home build micro-spectroscopy set-up built around a closed-cycle, low vibration attoDry cryostat with a temperature controller (T = 4 K–300 K). For PL, a HeNe laser (633 nm) was used for excitation (typical excitation power of 5 μW). The white light source for reflectivity measurements is a halogen lamp with a stabilized power supply. The emitted and/or reflected light was dispersed in a spectrometer and detected by a Si-CCD (charge-coupled device) camera. The excitation/detection spot diameter is ~1 μm.

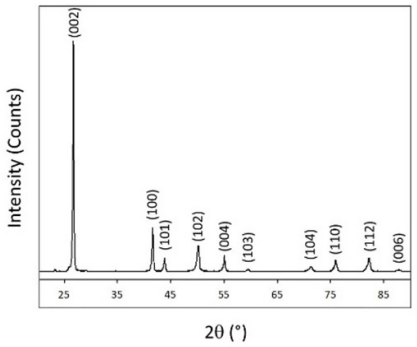

Figure 1. XRD pattern recorded on as-sintered hBN crystals.

3. Results and discussion

3.1. Synthesis and characterization

A mix of preceramized polyborazilene with a large amount of Li_3N (35 w%) is introduced in a BN crucible and placed into the pressure-controlled furnace. With standard conditions applied (1800 °C, 180 MPa, 8 h), hBN single crystals are formed. Actually, the use of the Li–B–N ternary system promotes the crystallization of large hBN crystals in a liquid phase [19]. XRD performed on the as-obtained samples (figure 1) evidences that the crystalline structure is in perfect agreement with the expected pattern for hBN (JCPDS 73-2095). The extreme thinness of the peaks (full width at half maximum (FWHM) = 3.6×10^{-3} rad^{-1}), sign of high crystal quality, does not allow interpretation by the Debye–Scherrer method as it does not apply for crystallite sizes over 200 nm [24].

These as-obtained crystals can be easily separated into independent flakes by simply using a tweezer. Their lateral size can reach the millimeter, as proven by optical (figure 2(a)) and scanning electron (figure 2(b)) images.

The uniform crystal orientation of these flakes is demonstrated by means of XRD (figure 3) that only shows hBN (002) and (004) reflections, suggesting a perfect in-plane arrangement of the hBN layers along the (002) direction.

Furthermore, Raman spectroscopy measurements displayed in figure 4 evidence a two-phonon mode as expected for hBN crystals: an intense mode at high-frequency (1366.1 cm^{-1}) (figure 4(b)) which corresponds to the in-plane E_{2g} optical phonon peak, and a second one in the low frequency region, at 52.6 cm^{-1} (figure 4(a)) attributed to the rigid shearing oscillation between adjacent layers, which is consistent with previously reported [25–27]. Corresponding FWHM values of, respectively 7.6 and 1.3 cm^{-1} are among the smallest reported in the literature for non mono-isotopic hBN [28, 29] indicating, again, a hBN source of high quality.

XPS general survey recorded on a typical hBN flake is presented in figure 5. The chemical composition determined with an x-ray beam of about 100 μm before and after a 2 μm Ar^+ etching (inset figure 5) indicates that surface contamination with oxygen (O1s, 532 eV) and carbon (C1s, 283 eV) is reduced down to XPS detection limit after etching, and that only expected boron (B1s, 189 eV) and nitrogen (N1s, 397 eV) species are remaining.

Furthermore, the B/N ratio of 0.99 measured on the raw surface indicates that the BN stoichiometry is as close to 1:1 as XPS can accurately measure. It is to be noted that XPS is a large-scale measurement (100 μm) and is not able to provide insight on crystal defects or local stoichiometry mismatch. As a reminder, since a preferential sputtering of nitrogen atoms occurs during the Ar^+ sputtering process, the B/N ratio cannot be used for quantitative composition analysis after etching. Moreover, the presence of π plasmon loss peaks at ~9 eV away from the B1s and N1s peaks is consistent with the sp^2 character of the chemical bonding within the layers [30, 31].

Since XRD and Raman spectroscopy have proven their limitations for comparing high quality hBN single crystals [32], CL experiments were performed in a dedicated scanning electron microscope. A spectral calibration of the detection system was performed to correct the CL spectra from the low sensitivity in the UV range [22].

Figure 6(a) shows the CL spectrum at room temperature taken from a part of a hBN crystal. The spectrum is dominated by the intrinsic radiative recombination of hBN, i.e. free exciton recombination with a maximum near 215 nm. A weak defect band related to carbon impurities is also detected with zero phonon line at 302 nm. Taniguchi *et al* tried to correlate this signal to the impurity concentration in hBN crystals by voluntarily degrading them [9]. Hence, contamination is here expected to be close to the detection limit of secondary ion mass spectrometry but no precise quantification can be provided. The measurement of the free exciton lifetime by time

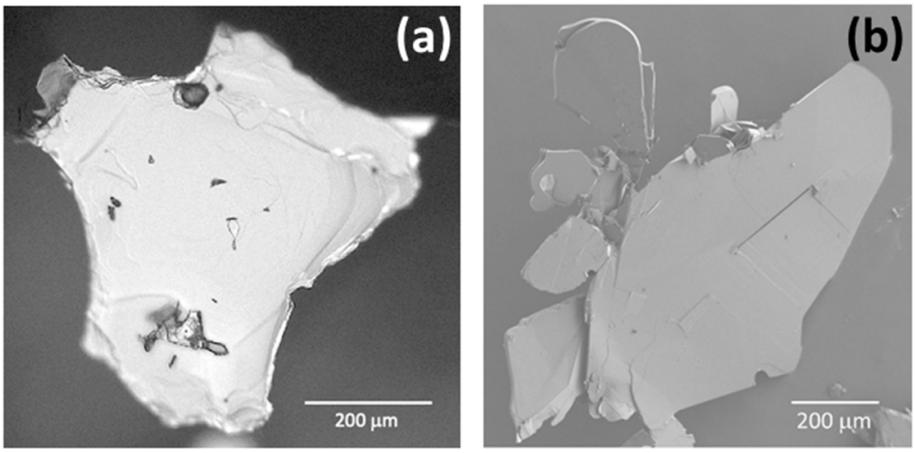

Figure 2. (a) Optical and (b) scanning electron microscopy images showing hBN flakes with lateral sizes up to millimeter.

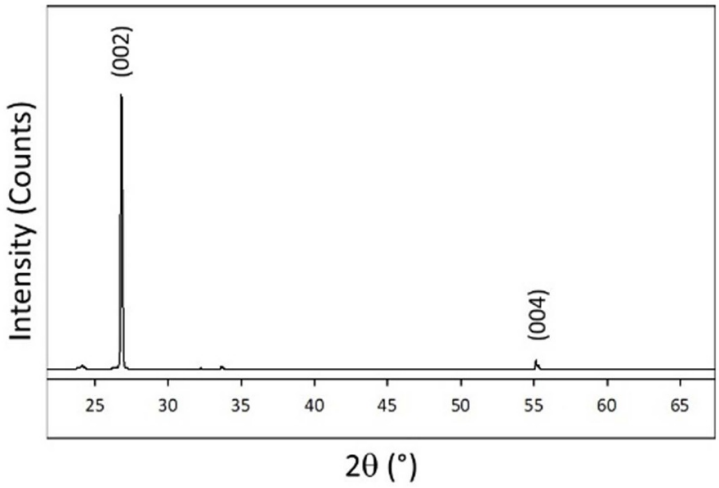

Figure 3. XRD pattern recorded on the h-BN flakes on the silicon holder.

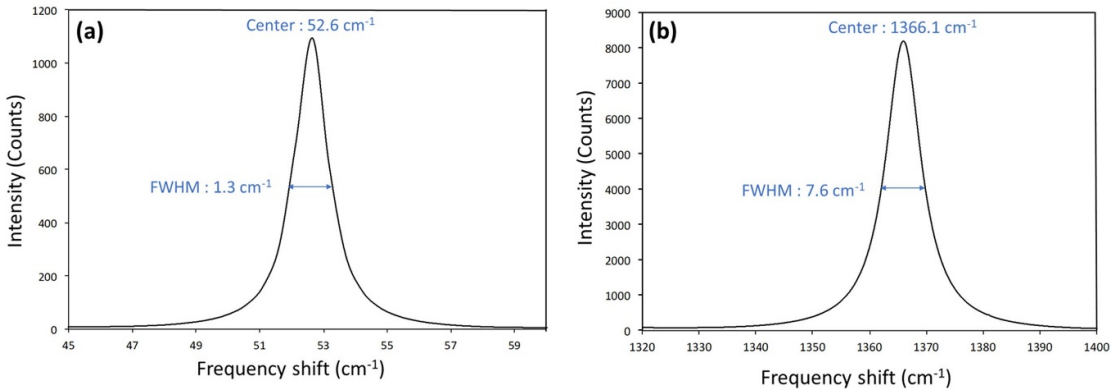

Figure 4. Raman spectra recorded on the hBN fragments at low (a) and high (b) frequencies.

resolved CL [33] provides a meaningful benchmarking basis of the samples with HP/HT [10] and AP/HT [34, 35] crystals. The free exciton lifetime was found at 0.43 ns, which indicates that the quality is lower in terms of purity or crystalline defects than in HP/HT crystals (4.2 ns) but remains comparable to AP/HT ones (0.1–1.1 ns). Again, no quantification is accessible using this measurement yet.

Figure 6(b) shows a high-resolution spectrum acquired at 10 K in the UV region of exciton

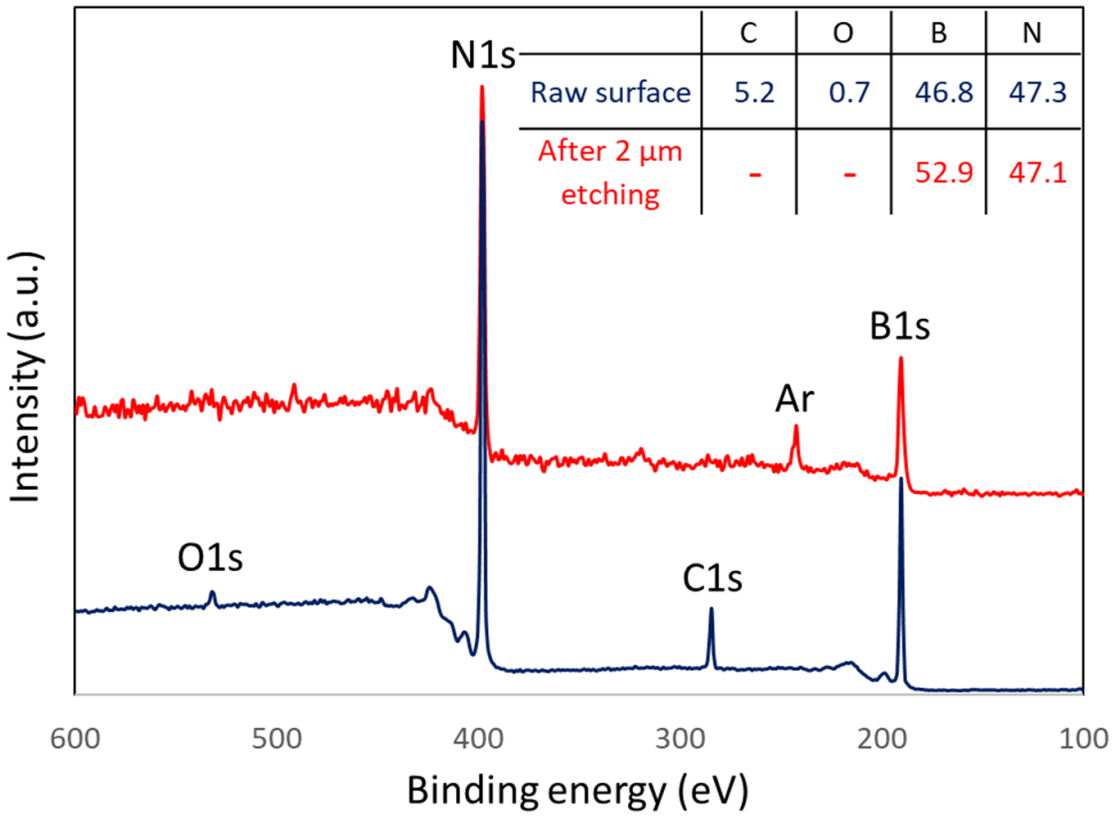

Figure 5. XPS general survey and elemental composition (inset) of hBN flake before (blue) and after (red) a 2 μm Ar^+ surface etching.

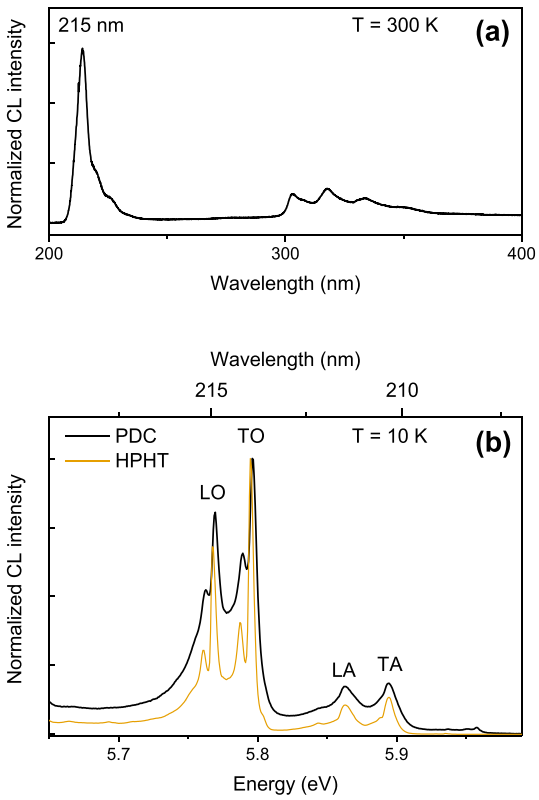

Figure 6. (a) CL spectrum at room temperature recorded on a hBN crystal; (b) high resolution CL spectrum at low temperature showing the free exciton recombinations assisted with different phonons. Both spectra are corrected from the spectral sensitivity of the detection system in the UV. A spectrum from a HP/HT hBN reference sample is shown for comparison.

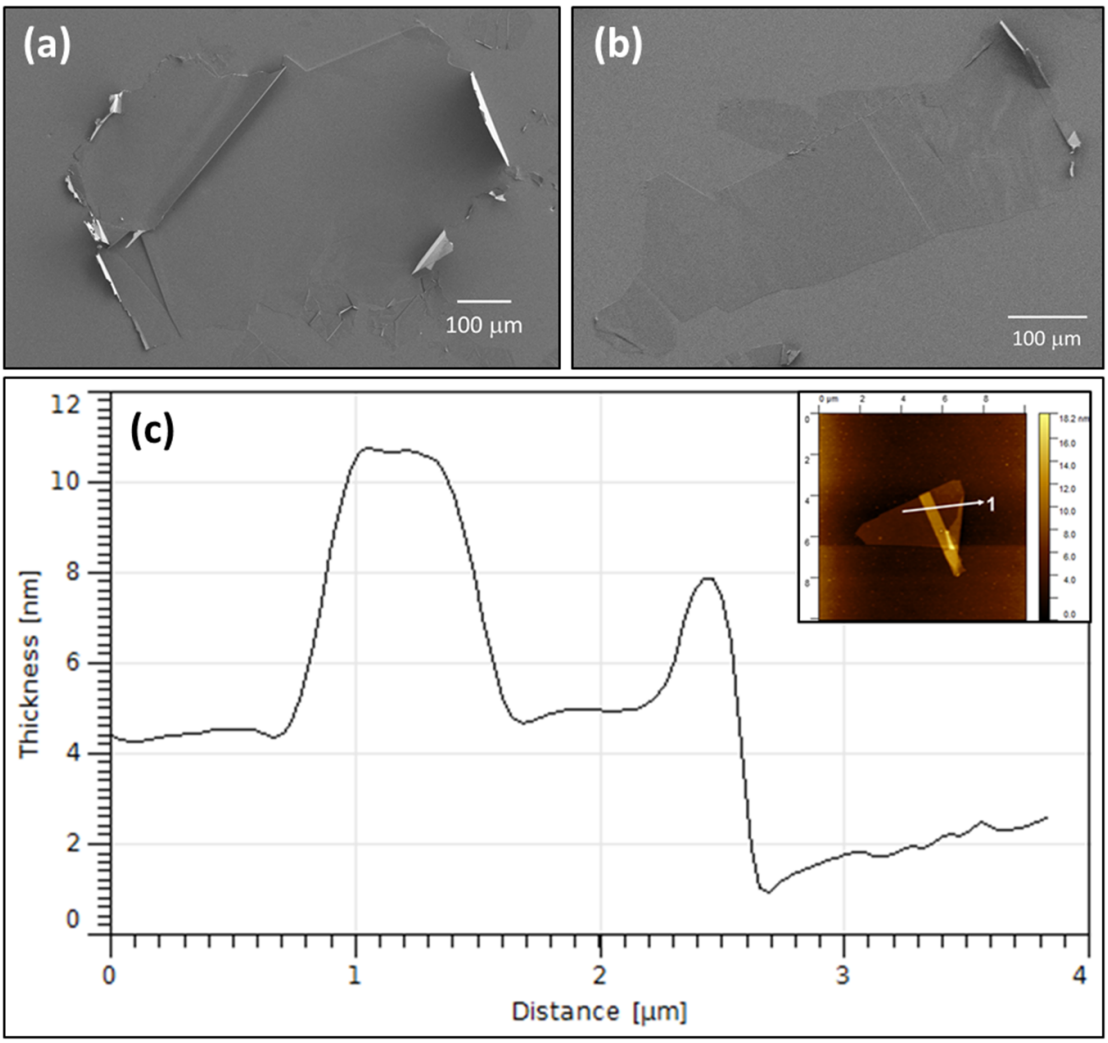

Figure 7. (a) and (b) SEM images of BNNSs of a few hundreds of microns as lateral size; (c) AFM profile obtained on BNNSs (inset).

recombinations. The phonon-assisted recombinations of the indirect exciton of hBN are clearly resolved and identified as TO, LO, TA and LA phonons. The peak linewidths are comparable to the reference hBN HP/HT crystals, plotted for comparison. These results indicate a fair quality of the hBN crystals given the soft chemical method used here.

In summary, XRD, Raman, and XPS characterization techniques lead to the same conclusion: both the crystallinity and purity of the flakes extracted from crystals grown by PDC/PCS are identical to the HP/HT reference crystals. Here, we reach the resolution limit of each characterization technique applied to hBN. CL is becoming the reference characterization technique for high quality hBN and indeed it shows residual defects attributed to carbon contamination higher than for HP/HT crystals, inducing lower exciton lifetime. The strong intrinsic radiative recombination is however very close to the HP/HT results.

In order to give an insight on PDC/PCS hBN quality and purity, and to prove that this material shows comparable properties to HP/HT crystals, optical devices were fabricated. Here we consider the encapsulation of two different TMDs with BNNSs exfoliated from PDC/PCS hBN.

The hBN flakes have been exfoliated into BNNSs using a PDMS dry transfer and deposited onto an oxidized silicon substrate (285 nm thick SiO_2). SEM observations show the exfoliation efficiency since the BNNSs keep lateral dimensions of more than hundreds of microns (figures 7(a) and (b)) while their thickness is reduced to 2.5–4 nm, which corresponds to 7–12 stacked layers as proven by AFM (figure 7(c)).

3.2. van der Waals heterostructures

Seven devices of $MoSe_2$ and WSe_2 MLs encapsulated into BNNSs have been fabricated by mechanical exfoliation and stamping. The bottom (top) hBN thicknesses in the hBN/TMD ML/hBN van der Waals heterostructures are typically in the range 100–200 nm (10–20 nm) respectively. These values can be roughly determined using the color observed in optical microscopy experiments. As shown in a

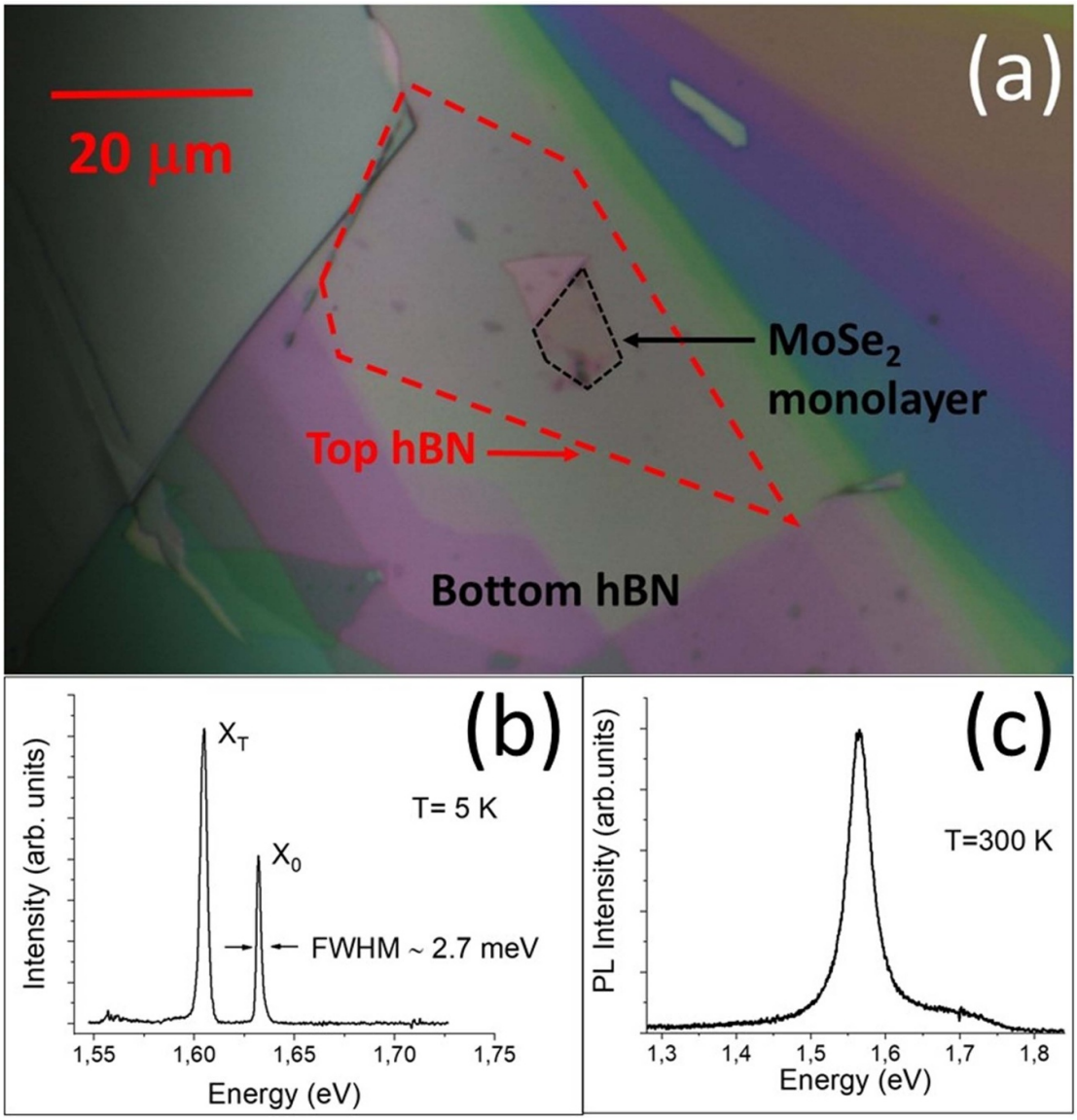

Figure 8. $MoSe_2$ ML—(a) optical microscope image of the hBN/$MoSe_2$ ML/hBN heterostructure; PL spectrum measured at (b) $T = 5$ K and (c) $T = 300$ K.

previous work, this method gives similar results to AFM measurements [36].

Their properties have been investigated by optical spectroscopy and they exhibit similar properties. We show the results on two of them, one based on $MoSe_2$ and the other one on WSe_2, in figures 8 and 9 respectively. Figure 8(a) shows an optical microscopy image of the fabricated van der Waals heterostructure hBN/$MoSe_2$/hBN. Figure 8(b) presents the PL spectrum for a hBN/$MoSe_2$ ML/hBN structure at $T = 5$ K. It evidences clearly two narrow peaks corresponding respectively to the recombination of neutral exciton (X_0) and charged exciton (X_T), in agreement with previous reports [4, 5]. Remarkably the PL linewidth of both lines is very narrow. The FWHM of the neutral exciton line is ~2.7 meV, demonstrating the very high quality of the structure using BNNSs as encapsulation layers. Comparable linewidths are obtained with HP/HT hBN encapsulation [4, 5, 37, 38]. It is worth mentioning that non-encapsulated TMD MLs are usually characterized by PL linewidths of a few tens of meV due to the dielectric disorder around the TMD ML [8, 39]. One can notice in figure 8(b) a rather large intensity of the charged exciton PL (larger than the one usually obtained with HP/HT crystals), indicating a possible doping effect of the TMD ML induced by the BNNS material. Figure 8(c) displays the PL spectrum measured at room temperature with a linewidth of about 39 meV, indicating a small inhomogeneous contribution as a consequence again of the high quality of encapsulation of the TMD ML with BNNSs.

In order to test the BNNSs encapsulation with another TMD material, we have investigated the properties of hBN/WSe_2 ML/hBN structures. Figure 9 presents the differential reflectivity spectrum measured at low temperature ($T = 5$ K). It exhibits two narrow resonances at 1.721 and 1.854 eV,

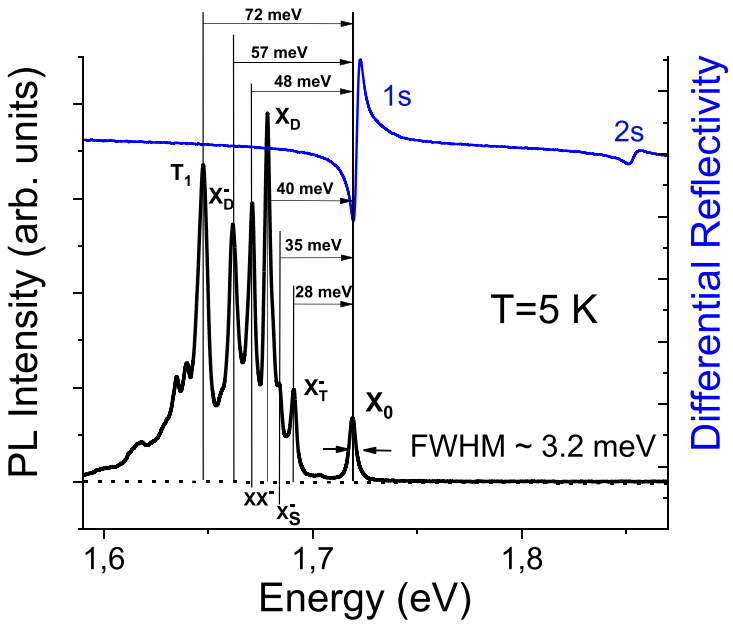

Figure 9. WSe_2 ML—differential reflectivity (right axis) and PL spectra of the hBN/WSe_2 ML/hBN heterostructure measured at $T = 5$ K.

corresponding to the neutral exciton X_0 ground state (1 s) and excited state (2 s) respectively. The observation of the exciton excited state attests to the high quality of the structure. Figure 9 also displays the measured PL spectrum. At high energy, we observe the neutral exciton line X_0, characterized by a line width of 3.2 meV (FWHM). This narrow linewidth is comparable with that measured on the best samples made with HP/HT hBN encapsulation [40]. At lower energy, several narrow peaks are also clearly visible in figure 9. We emphasize that these PL lines are not due to recombination involving defects but correspond to the radiative recombination of different exciton complexes as already identified in WSe_2 MLs encapsulated with HP/HT hBN [41–43]. The peaks lying 28 and 35 meV below X_0 correspond to the recombination of the triplet (X_T) and singlet (X_S) charged excitons respectively [44]. The dark neutral exciton (X_D) lies 40 meV below X_0 [40] whereas the charged biexciton XX^- and the dark charged excitons $X_D{}^-$ recombine with an energy 48 and 57 meV below X_0 respectively [45]. Finally the T_1 peak, lying 72 meV below X_0, has not yet been identified but it is also observed in WSe_2 MLs encapsulated with HP/HT boron nitride [41]. The clear observation of all these exciton complexes in PL spectroscopy is again a proof of the excellent quality of the samples obtained with BNNSs encapsulations. Similar to the results for $MoSe_2$ MLs, the detection of charged exciton complexes demonstrates that the ML is slightly doped. The observation of the two trions proves that this doping is of N type (because of the specific band structure of the TMDs, only one type of charged exciton can be observed in the case of a P type doping). In comparison with the PL spectra measured in charge adjustable WSe_2 MLs [41], we can infer that the doping density is typically of the order of 10^{11} cm^{-2}. Finally, we have carefully checked that the laser excitation of the BNNSs only (without any TMDs) does not yield any luminescence due to defect recombination in the visible region of the spectrum. This is an additional proof of the high quality of the BNNSs obtained with the polymer route, which confirms other positive results recently obtained on metal–hBN–metal capacitor devices [46].

4. Conclusion

In this work, it has been demonstrated that the reported disruptive polymer derived ceramics route coupled with a pressure-controlled sintering has been efficiently employed for the synthesis of millimeter-scale hBN crystals. The current process requires softer conditions, is considerably faster, less energy consuming and scalable. The high crystalline and chemical quality of these crystals is attested by different complementary conventional characterization techniques including XRD, Raman spectroscopy and XPS. All these methods lead to the same conclusion, namely that the quality of resulting crystals is comparable to that obtained by the HP/HT or AP/HT growth processes. CL was able to distinguish between HP/HT and PDC/PCS samples. It shows defects attributed to low level carbon contamination. Importantly, the good characteristics of these crystals are preserved after exfoliation, opening the way to the use of the extracted BNNSs for fabricating diverse devices. In this work we have used the optical properties of the TMD ML as a complementary probe of the quality of the BNNSs. As a proof of concept, we showed a

first successful application in van der Waals heterostructures made of $MoSe_2$ and WSe_2 MLs encapsulated into PDC/PCS BNNSs. The PL of TMDC layers evidences exciton complexes proving the excellent quality of the encapsulated material very comparable to HP/HT hBN.

Data availability statement

All data that support the findings of this study are included within the article (and any supplementary files).

Acknowledgments

The authors thank the CLYM, for providing access to the SEM facilities, CECOMO for access to Raman spectroscopy and Science et Surface (Ecully, France) for XPS analyses.

This work has been partially financially supported by the European Union Horizon 2020 Program under the Graphene Flagship (Graphene Core 3, Grant No. 881603), the iMUST LABEX program MUSCAT-2D and the National Research Agency, France (project ELuSeM n° ANR-21-CE24-0025). Y Li acknowledges the China Scholarship Council (CSC) for the PhD Grant support.

ORCID iDs

Camille Maestre https://orcid.org/0000-0002-7911-3758
Yangdi Li https://orcid.org/0000-0002-8515-7802
Vincent Garnier https://orcid.org/0000-0003-0607-4409
Philippe Steyer https://orcid.org/0000-0003-0835-9862
Sébastien Roux https://orcid.org/0000-0001-6493-744X
Annick Loiseau https://orcid.org/0000-0002-1042-5876
Julien Barjon https://orcid.org/0000-0003-1749-2980
Cedric Robert https://orcid.org/0000-0002-3722-3705
Xavier Marie https://orcid.org/0000-0002-7772-2517
Catherine Journet https://orcid.org/0000-0002-3328-317X
Berangere Toury https://orcid.org/0000-0001-5889-0796

References

[1] Vuong T Q P *et al* 2017 Deep ultraviolet emission in hexagonal boron nitride grown by high-temperature molecular beam epitaxy *2D Mater.* **4** 021023
[2] Jiang H X and Lin J Y 2014 Hexagonal boron nitride for deep ultraviolet photonic devices *Semicond. Sci. Technol.* **29** 084003
[3] Rigosi A F, Levy A L, Snure M R and Glavin N R 2021 Turn of the decade: versatility of 2D hexagonal boron nitride *J. Phys. Mater.* **4** 032003
[4] Cadiz F *et al* 2017 Excitonic linewidth approaching the homogeneous limit in MoS_2-based van der Waals heterostructures *Phys. Rev.* X **7** 021026
[5] Ajayi O A *et al* 2017 Approaching the intrinsic photoluminescence linewidth in transition metal dichalcogenide monolayers *2D Mater.* **4** 031011
[6] Movva H C P, Fallahazad B, Kim K, Larentis S, Taniguchi T, Watanabe K, Banerjee S K and Tutuc E 2017 Density-dependent quantum hall states and Zeeman splitting in monolayer and bilayer WSe_2 *Phys. Rev. Lett.* **118** 247701
[7] Pisoni R *et al* 2018 Interactions and magnetotransport through spin-valley coupled landau levels in monolayer MoS_2 *Phys. Rev. Lett.* **121** 247701
[8] Raja A *et al* 2019 Dielectric disorder in two-dimensional materials *Nat. Nanotechnol.* **14** 832–7
[9] Taniguchi T and Watanabe K 2007 Synthesis of high-purity boron nitride single crystals under high pressure by using Ba–BN solvent *J. Cryst. Growth* **303** 525–9
[10] Watanabe K, Taniguchi T and Kanda H 2004 Direct-bandgap properties and evidence for ultraviolet lasing of hexagonal boron nitride single crystal *Nat. Mater.* **3** 404–9
[11] Zastrow M 2019 Meet the crystal growers who sparked a revolution in graphene electronics *Nature* **572** 429–32
[12] Maestre C, Toury B, Steyer P, Garnier V and Journet C 2021 Hexagonal boron nitride: a review on selfstanding crystals synthesis towards 2D nanosheets *J. Phys. Mater.* **4** 044018
[13] Li J *et al* 2020 Single crystal growth of monoisotopic hexagonal boron nitride from a Fe–Cr flux *J. Mater. Chem.* C **8** 9931–5
[14] Hoffman T B, Clubine B, Zhang Y, Snow K and Edgar J H 2014 Optimization of Ni–Cr flux growth for hexagonal boron nitride single crystals *J. Cryst. Growth* **393** 114–8
[15] Liu S, He R, Ye Z, Du X, Lin J, Jiang H, Liu B and Edgar J H 2017 Large-scale growth of high-quality hexagonal boron nitride crystals at atmospheric pressure from an Fe–Cr flux *Cryst. Growth Des.* **17** 4932–5
[16] Yuan S, Linas S, Journet C, Steyer P, Garnier V, Bonnefont G, Brioude A and Toury B 2016 Pure & crystallized 2D boron nitride sheets synthesized via a novel process coupling both PDCs and SPS methods *Sci. Rep.* **6** 20388
[17] Li Y, Garnier V, Journet C, Barjon J, Loiseau A, Stenger I, Plaud A, Toury B and Steyer P 2019 Advanced synthesis of highly crystallized hexagonal boron nitride by coupling polymer-derived ceramics and spark plasma sintering processes-influence of the crystallization promoter and sintering temperature *Nanotechnology* **30** 3
[18] Matsoso B, Hao W, Li Y, Vuillet-a-Ciles V, Garnier V, Steyer P, Toury B, Marichy C and Journet C 2020 Synthesis of hexagonal boron nitride 2D layers using polymer derived ceramics route and derivatives *J. Phys. Mater.* **3** 034002
[19] Li Y, Garnier V, Steyer P, Journet C and Toury B 2020 Millimeter-scale hexagonal boron nitride single crystals for nanosheet generation *ACS Appl. Nano Mater.* **3** 1508–15
[20] Yuan S, Toury B, Journet C and Brioude A 2014 Synthesis of hexagonal boron nitride graphene-like few layers *Nanoscale* **6** 7838–41
[21] Castellanos-Gomez A, Buscema M, Molenaar R, Singh V, Janssen L, van der Zant H S J and Steele G A 2014 Deterministic transfer of two-dimensional materials by all-dry viscoelastic stamping *2D Mater.* **1** 011002
[22] Schué L, Sponza L, Plaud A, Bensalah H, Watanabe K, Taniguchi T, Ducastelle F, Loiseau A and Barjon J 2019 Bright luminescence from indirect and strongly bound excitons in H-BN *Phys. Rev. Lett.* **122** 067401
[23] Schué L, Berini B, Betz A C, Plaçais B, Ducastelle F, Barjon J and Loiseau A 2016 Dimensionality effects on the luminescence properties of HBN *Nanoscale* **8** 6986–93

[24] Cullity B D and Stock S R 2001 *Elements of X-ray Diffraction* 3rd edn (Upper Saddle River, NJ: Prentice-Hall)
[25] Kuzuba T, Era K, Ishii T, Sato T and 1978 A low frequency Raman-active vibration of hexagonal boron nitride *Solid State Commun.* **25** 863–5
[26] Pakdel A, Bando Y and Golberg D 2014 Nano boron nitride flatland *Chem. Soc. Rev.* **43** 934–59
[27] Stenger I, Schué L, Boukhicha M, Berini B, Plaçais B, Loiseau A and Barjon J 2017 Low frequency Raman spectroscopy of few-atomic-layer thick HBN crystals *2D Mater.* **4** 031003
[28] Gorbachev R V *et al* 2011 Hunting for monolayer boron nitride: optical and Raman signatures *Small* **7** 465–8
[29] Nemanich R J, Solin S A and Martin R M 1981 Light scattering study of boron nitride microcrystals *Phys. Rev.* B **23** 6348–56
[30] Berns D H and Cappelli M A 1996 Cubic boron nitride synthesis in low-density supersonic plasma flows *Appl. Phys. Lett.* **68** 2711–3
[31] Trehan R, Lifshitz Y and Rabalais J W 1998 Auger and x-ray electron spectroscopy studies of HBN, CBN, and $N^{+}{}_{2}$ ion irradiation of boron and boron nitride *J. Vac. Sci. Technol.* A **8** 4026
[32] Schué L, Stenger I, Fossard F, Loiseau A and Barjon J 2017 Characterization methods dedicated to nanometer-thick HBN layers *2D Mater.* **4** 015028
[33] Roux S *et al* 2021 Radiative lifetime of free excitons in hexagonal boron nitride *Phys. Rev.* B **104** L161203
[34] Liu S, He R, Xue L, Li J, Liu B and Edgar J H 2018 Single crystal growth of millimeter-sized monoisotopic hexagonal boron nitride *Chem. Mater.* **30** 6222–5
[35] Kubota Y, Watanabe K, Tsuda O and Taniguchi T 2007 Deep ultraviolet light-emitting hexagonal boron nitride synthesized at atmospheric pressure *Science* **317** 932–4
[36] Fang H H *et al* 2019 Control of the exciton radiative lifetime in van der Waals heterostructures *Phys. Rev. Lett.* **123** 067401
[37] Rogers C, Gray D, Bogdanowicz N, Taniguchi T, Watanabe K and Mabuchi H 2020 Coherent feedback control of two-dimensional excitons *Phys. Rev. Res.* **2** 012029
[38] Zhou Y *et al* 2020 Controlling excitons in an atomically thin membrane with a mirror *Phys. Rev. Lett.* **124** 027401
[39] Wang G, Gerber I C, Bouet L, Lagarde D, Balocchi A, Vidal M, Amand T, Marie X and Urbaszek B 2015 Exciton states in monolayer $MoSe_2$: impact on interband transitions *2D Mater.* **2** 045005
[40] Wang G *et al* 2017 In-plane propagation of light in transition metal dichalcogenide monolayers: optical selection rules *Phys. Rev. Lett.* **119** 047401
[41] He M *et al* 2020 Exciton complexes in a monolayer semiconductor *Nat. Commun.* **11** 618
[42] Robert C *et al* 2021 Measurement of conduction and valence bands g-factors in a transition metal dichalcogenide monolayer *Phys. Rev. Lett.* **126** 067403
[43] Liu E, van Baren J, Liang C-T, Taniguchi T, Watanabe K, Gabor N M, Chang Y-C and Lui C H 2020 Multipath optical recombination of intervalley dark excitons and trions in monolayer WSe_2 *Phys. Rev. Lett.* **124** 196802
[44] Jones A M, Yu H, Schaibley J R, Yan J, Mandrus D G, Taniguchi T, Watanabe K, Dery H, Yao W and Xu X 2016 Excitonic luminescence upconversion in a two-dimensional semiconductor *Nat. Phys.* **12** 323–7
[45] Liu E, van Baren J, Lu Z, Altaiary M M, Taniguchi T, Watanabe K, Smirnov D and Lui C H 2019 Gate tunable dark trions in monolayer WSe_2 *Phys. Rev. Lett.* **123** 027401
[46] Pierret A *et al* 2022 Dielectric permittivity, conductivity and breakdown field of hexagonal boron nitride *Mater. Res. Express* (https://doi.org/10.1088/2053-1591/ac4fe1)